applied sciences

MDPI

Article

MRI Compatible Planar Material Acoustic Lenses

Daniel Tarrazó-Serrano [1], Sergio Castiñeira-Ibáñez [1], Eugenio Sánchez-Aparisi [2], Antonio Uris [1] and Constanza Rubio [1,*]

[1] Centro de Tecnologías Físicas, Universitat Politècnica de València, Camí de Vera s/n, 46022 València, Spain; dtarrazo@fis.upv.es (D.T.-S.); sercasib@upvnet.upv.es (S.C.-I.); auris@fis.upv.es (A.U.)
[2] Hospital Francesc de Borja, 46702 Gandia, València, Spain; sanchez_eug@gva.es
* Correspondence: crubiom@fis.upv.es

Received: 10 October 2018; Accepted: 13 December 2018; Published: 15 December 2018

Featured Application: Authors are encouraged to provide a concise description of the specific application or a potential application of the work. This section is not mandatory.

Abstract: Zone plate lenses are used in many areas of physics where planar geometry is advantageous in comparison with conventional curved lenses. There are several types of zone plate lenses, such as the well-known Fresnel zone plates (FZPs) or the more recent fractal and Fibonacci zone plates. The selection of the lens material plays a very important role in beam modulation control. This work presents a comparison between FZPs made from different materials in the ultrasonic range in order to use them as magnetic resonance imaging (MRI) compatible materials. Three different MRI compatible polymers are considered: Acrylonitrile butadiene styrene (ABS), polymethyl methacrylate (PMMA) and polylactic acid (PLA). Numerical simulations based on finite elements method (FEM) and experimental results are shown. The focusing capabilities of brass lenses and polymer zone plate lenses are compared.

Keywords: MRI; Zone Plates; ultrasonic lenses

1. Introduction

The development of modulating and focusing energy systems has been a field of study of great interest for scientist and engineers. The lens is a devices that is able to perform this energy modulation. Lenses allow beam forming, control propagation and focusing the energy that impinges on them. These effects are produced by refractive and diffractive phenomena. Transmission efficiency is one of the most important aspects, particularly when low impedance contrast is presented between the lens and the host medium. Due to the wide versatility of the lenses, they have been used in different areas. For example, they have been applied in sonochemistry [1], construction [2] and the pharmaceutical industry [3].

The acoustic lenses, depending on the physics involved in the beam formation, can be divided into different groups, including refractive lenses and diffractive lenses. One example of lenses based on the refraction phenomenon are sonic crystal lenses made of periodic distributions of rigid cylinders [4]. Due to the subsonic sound speed inside the crystal, these lenses act similar to those in optical systems. Another example of this typology of acoustic lenses are those which modify the refractive index using labyrinths. These type of lenses are the so-called Gradient-Index lenses [5–7].

The other subtype of lenses, based on the diffractive phenomenon, conducts its behavior on the constructive interferences of the pressure field. An example of these types of lenses is the fractal lenses, which are able to generate different foci depending on their fractal geometrical properties [8]. Fresnel Zone Plates (FZP) have an improved focusing capacity. Among the different ways to implement FZPs,

one of the most common and easiest is to alternate transparent and blocking zones, which results in a Soret type FZP [9]. To obtain these blocking areas, materials that are opaque to sound are required. This fact is accomplished by selecting materials that have a high impedance contrast with the host medium. There are studies that have implemented Soret FZP (SZP) by ultrasounds based on these type of lenses [10].

A material that has a high impedance with respect to water and that allows for the creation of opaque zones to achieve a Soret type lens is brass. However, this type of material has limitations, especially when used in fields such as bioengineering. The use of acoustic lenses in medicine for high intensity focused ultrasounds (HIFU) treatment is one of the current lines of research. magnetic resonance imaging (MRI) is the technique that is most used for guiding HIFU treatment [11].

MRI is a technique used for soft tissue structure imaging in a non-invasive way. The image is obtained by aligning and relaxing the magnetic moments of the atoms of the introduced elements in the MRI. Tissues are exposed to a strong external time-independent magnetic field. Thus, metallic elements cannot be introduced in the resonance zone due to their interference in the image and because they could damage MRI-systems. To avoid interaction with the electromagnetic field, non-metallic materials should be used in the construction of lenses. One of these materials is polylactic acid (PLA) [12]. The MRI environment requires materials such as PLA for medical instruments and patient supports. Recently, PLA has been used for this purpose and its reliability has been shown [13]. The HIFU transducer is embedded within a specially designed table that fits into the MRI device. This integrated system, has a degassed water bath where the transducer is located. The patient lies over this system on [14]. Although the transducer and the lens must be immersed in this water bath, degradation of the PLA will occur over long-term immersion. PLA degrades in water after a period ranging from months to a year [15]. Therefore it must be taken into account that, in MRI systems, the lens and the transducer are not permanently submerged. After 20 to 25 min, the system is extracted from the water bath, and for this reason, the time of degradation due to being immersed in water can be prolonged considerably.

In this work, three lenses with three types of compatible materials with MRI environments are compared. In this sense, acrylonitrile butadiene styrene (ABS), polymethyl methacrylate (PMMA) and polylactic acid (PLA) materials are used. Furthermore, a SZP built in brass is compared. Although, this material is not MRI compatible, it is the nearest to the ideal SZP that can be implemented in real projects. In the comparison, a not compatible with MRI lens built in brass and an ideal Soret lens will be added. Results are obtained and compared both numerically and experimentally. Numerical results have been obtained using the commercial software COMSOL Multiphysics 4.3a by COMSOL Inc. (Sweden) [16]. In this work, it has been verified that the ratio of the transmission capacity that is related to the ratio of impedances of the medium and the lens, directly influences the focusing capacity.

2. Methodology and Theoretical Analysis

Fresnel zone plates are circular concentric structures, which are known as Fresnel regions. Every consecutive region has a π phase shift between them. This fact makes a coherent contribution to obtain high intensity levels at focal length (F_L), which is the location in the axial coordinate where the focus is placed. The number of Fresnel regions is defined as N, this includes both opaque and transparent acoustic sections. The working frequency is defined as f_0 and radial distances (r_n) of each Fresnel zone can be obtained using Equation (1) valid for plane wave incidence.

$$r_n = \sqrt{n\lambda F_L + \left(\frac{n\lambda}{2}\right)^2} \qquad n = 1, 2, ..., N \tag{1}$$

In this work, underwater transmission is considered and lenses are designed for ultrasound applications. Therefore, piston sources have to be considered when FZPs are implemented. Due to spherical wave incidence consideration, Equation (2) has been used where d is the separation between the point source and the lens.

$$d + F_L + \frac{n\lambda}{2} = \sqrt{d^2 + r_n^2} + \sqrt{F_L^2 + r_n^2} \tag{2}$$

The acoustic wave has to propagate through the host medium, then cross Fresnel regions and afterwards continue through the host medium. A three-layer configuration has to be considered (Figure 1). Acoustic impedance (Z) is defined as the product of the medium density (ρ) and the sound propagation velocity (c) in it. Therefore, it is necessary to consider the input (Z_{in}) and output (Z_{out}) acoustic impedance and the transmission pressure coefficients must be calculated (t). This coefficient is a clear indicator of the blocking capacity of the elements of the FZP. Hence, t is defined as the relation between the transmitted field and the incident field. Density (ρ), sound propagation velocity (c) and acoustic impedance (Z_{mat}) values have been shown in Table 1. Using these values in Equation (3), Z_{in} could be obtained [17].

$$Z_{in} = Z_{mat} \frac{Z_{out} + jZ_{mat} \tan(k_{mat} d)}{Z_{mat} + jZ_{out} \tan(k_{mat} d)} \tag{3}$$

where k_m is the wave number, defined as $k_m = \omega / c$. Considering $\omega = 2\pi f_0$. Once Z_{in} is obtained, reflection coefficient is defined in Equation (4).

$$r_{in} = \frac{Z_{in} - Z_{water}}{Z_{in} + Z_{water}} \tag{4}$$

The equation that relates the field balance as a function of the impedance and reflection coefficient of the system is defined in Equation (5) and gives t values depending on the material.

$$|t| = \frac{|p_t^+|}{|p_{in}^+|} = \sqrt{(1 - |r_{in}|^2)} \tag{5}$$

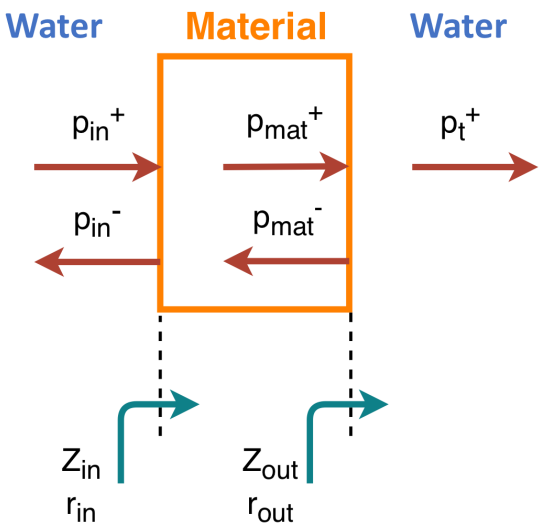

Figure 1. Transmission diagram of the implemented lenses.

Table 1. Density and sound speed values. Acrylonitrile butadiene styrene (ABS), polylactic acid (PLA), and polymethyl methacrylate (PMMA).)

Material	ρ (kg/m^3)	c (m/s)	$Z_{mat}(Rayls)$	Z_{mat}/Z_{water}
ABS	1050	2250	$2.4{\cdot}10^6$	1.58
PLA	1240	2220	$2.8{\cdot}10^6$	1.84
PMMA	2690	1191	$3.2{\cdot}10^6$	2.14
Brass	8400	4700	$39.5{\cdot}10^6$	26.32
PLA-Air-PLA	398	944	$3.6{\cdot}10^5$	0.25

Considering the transmission coefficient values obtained (0.23 for brass, 0.51 for PLA-Air-PLA and more than 0.95 for ABS, PLA and PMMA), it can be affirmed that full implemented MRI compatible material lenses will focus less energy at the F_L if it is compared to brass FZP or ideal SZP. Therefore, one solution is proposed to obtain the desired impedance contrast. A FZP that includes an air chamber inside the structure has been implemented by using a 3D-printer. Thus, both lenses, full-PLA and air-chamber, have been compared.

2.1. Numerical Model

The finite elements method (FEM) has been used to obtain a numerical solution of the physical problem. The finite elements method allows us to study the physical phenomena involved in the interaction of waves with FZPs. Therefore, a mathematical model that replicates the conditions of the problem has been implemented. This method also allows us to determine the pressure distribution of the diffracted fields generated by the FZP when there is a piston emitter, causing interference phenomena. From the mesh generated by FEM, a partial differential equation solution is obtained for each node [18]. In this case, acoustic Helmholtz equation is considered (Equation (6)). To solve the Helmholtz equation, standard values of water such as density of the medium (ρ =1000 kg/m^3) and sound propagation velocity (c = 1500 m/s) have been considered. The working frequency of the FZPs is 250 kHz and it can be found by its relation with the angular velocity (ω). Finally, p corresponds to the acoustic pressure.

$$\nabla \cdot \left(-\frac{1}{\rho_0} (\nabla p) \right) = \frac{\omega^2 p}{\rho_0 c^2} \tag{6}$$

If a 3D model is considered, this will require high computational resources. To simplify the model and reduce this computational cost, as shown in previous works [19,20], the geometrical properties of the model are used taking advantage of its axisymmetry. Therefore, the model is simplified by implementing a semi-lens only. A complete solution is obtained by rotating it from its symmetry axis. This procedure achieves a reduction of the degrees of freedom necessary to obtain the results of the numerical simulation and thus significantly diminishing the calculation time.

The boundary conditions defined in the numerical models are explained below as seen in Figure 2. The contours of the model are defined as wave radiation condition boundary to emulate an infinitely large medium and therefore the Sommerfeld condition is satisfied. Acoustic impedance domain definition has been used for all opaque Fresnel regions for each lens. In the case of the SZP lens, the contours are considered infinitely rigid, applying the Neumann condition (the sound velocity in the contour is zero).

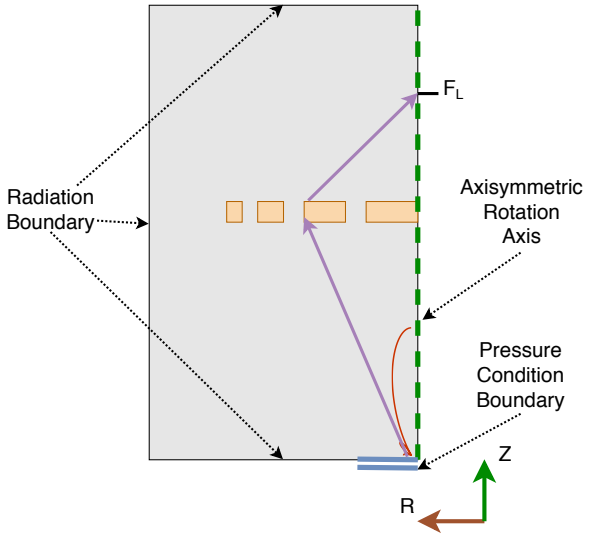

Figure 2. Scheme of the finite element method (FEM) conditions.

3. Experimental Set-Up

It is required to validate the results obtained from the theoretical models with other solutions such as numerical models and experimental measurements. In this sense, obtaining experimental results is fundamental to validate the numerical models. A complex measurement and acquisition system is needed to perform the experiments given the technical difficulties to control the underwater devices. The Center for Physics Technologies: Acoustics, Materials and Astrophysics of the Universitat Politècnica de València has a robotized and automated system for high precision ultrasound measurements. The robot is built based on the size of the immersion tank where the tests and experiments are carried out, which contains distilled and degassed water, with dimensions of 0.5 m wide by 0.5 m high by 1 m long. These dimensions suppose that the immersion tank must contain around 200 L of distilled water to be functional, and allow both transducers and devices to be completely submerged, and avoid reflections due to the impedance changes produced by the change medium.

The measurement system is composed by a fixed emitter and a hydrophone coupled to the robotic system. This system obtains reliable and precise results that allow for the evaluation of the acoustic phenomena involved in these types of lenses. A plane immersion piston transducer built by Imasonic with 250 kHz of central working frequency and an active diameter of 32 mm has been used as the emitter. Also, a Precision Acoustics hydrophone, model 1.0 mm Needle Hydrophone is used as the receiver. This hydrophone is capable of measuring high frequencies, even if they have a very weak signal level. The sensitivity of the hydrophone is 850 nV/Pa (-241.4 dB 1V/µPa) with a tolerance of ± 3 dB. The frequency response is flat ± 2 dB between 3 and 12 MHz and ± 4 dB between 200 kHz and 15 MHz. The bandwidth ranges from 5 kHz to 15 MHz. Figure 3 shows an experimental set-up in a measurement. Two types of different configurations are used to generate and amplify the signals. The first one is to use an external function generator connected to a high power amplifier. The second configuration is to use a pulse generator (5077PR of Panametrics) with integrated amplifier. This generator and amplifier allows generating pulses with frequencies between 100 kHz and 20 MHz, a pulse repetition frequency (PRF) from 100 Hz to 5 kHz and a pulse amplitude between 100 and 400 V.

Figure 3. Experimental set-up.

All the results shown below are obtained for a working frequency of 250 kHz. For the experimental comparison, three lenses have been implemented, two made of PLA and one of brass. Every lens considered in this work was designed with 11 Fresnel zones and an outer radius of 88.8 mm. The thickness of the brass lens was 1 mm. For manufacturing reasons, the rest of the lenses had a total thickness of 5 mm. Figure 4 shows both PLA and brass lenses. Both PLA lenses are identical, the only difference being an inner air chamber to achieve a higher impedance contrast. As described in the previous section, it is not possible to differentiate them by the naked eye.

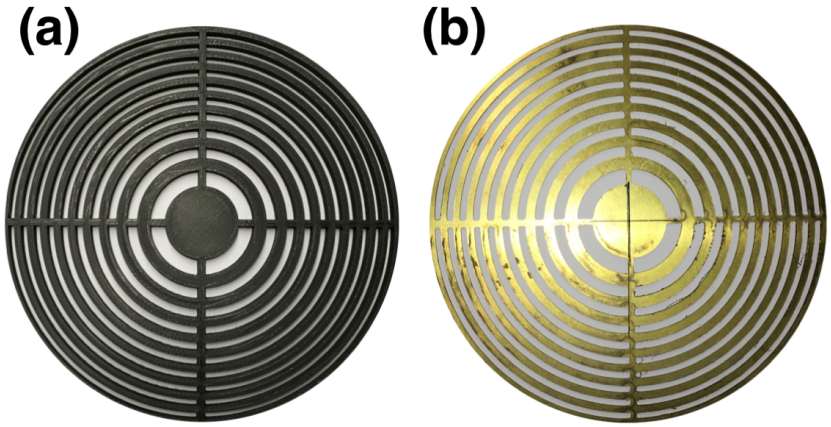

Figure 4. Implemented lenses, (**a**) PLA and (**b**) brass.

4. Results

Intensity gain for longitudinal axis cuts and maps have been calculated to compare all the lenses coherently. One parameter, which can be used to evaluate the focusing capacity of a lens is the intensity gain (G). The intensity gain is related with the intensity with both the intensity with lens (I) and intensity without lens (I_0), as shown in Equation (7).

$$G(dB) = 10 \cdot \log_{10}(I/I_0) \tag{7}$$

Intensity gain values have been calculated from Equation (7). Figure 5, shows the intensity gain for longitudinal cuts on the Z axis for both, numerical and experimental results. It can be seen from Figure 5a, that higher impedance contrast, as in the case of the ideal SZP or brass FZP lens, gives rise to a higher gain levels. As expected, the lower gains are obtained with those materials with impedance contrast values between 1 and 2 and for impedance contrast values lower than 1, the intensity gain increases. ABS, PLA, PLA-Air-PLA, and PMMA polymers, according with the values showed in Table 1, are not able to achieve enough intensity gain as brass FZP. By comparing the experimental results obtained for brass and PLA (see Figure 5b) with numerical ones (see Figure 5a) it can be seen that there is a good agreement. From Figure 5b, it is observed that the air chamber PLA lens has higher intensity gain than full PLA lens. This fact can be explained by the introduction of an air

layer. This layer, due to its low acoustic impedance, can block the transmission of the ultrasonic waves approaching its behavior to an ideal SZP. Nevertheless, a focal length displacement of 1.66λ is observed in the FZP lens built with air chamber and PLA. In this case, the displacement is due to the new three-layer configuration (PLA-Air-PLA). The resolution of the 3D-printer and the wall width needed to avoid porosities means that there is an interface between the host medium and the air chamber.

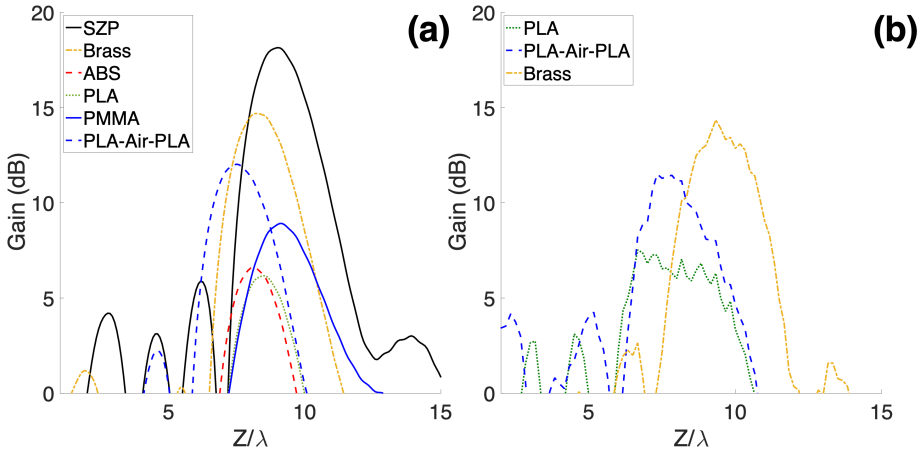

Figure 5. Intensity gain longitudinal cuts for (**a**) FEM results and (**b**) experimental results.

Figure 6 shows four intensity gain maps, the first three obtained experimentally and the fourth numerically. The experimental ones correspond to PLA, PLA-Air-PLA and brass, while the numerical one has been obtained using an ideal SZP. It has been verified how the results obtained with brass resembles the ideal SZP. This is due to the rigidity of the material. On the other hand, in PLA lens results, a diminishing intensity gain is observed. This intensity gain level can be improved using a PLA-Air-PLA lens. All the lenses are designed with a focal length located at 8.33λ for a working frequency of 250 kHz. When the lens is able to block destructive interference, it is possible to locate the focus in F_L. This occurs in brass and the ideal SZP case. Resulting from the lack of blocking capability, the full PLA FZP could not impede the incident pressure wave transferal generating aberrations in the F_L.

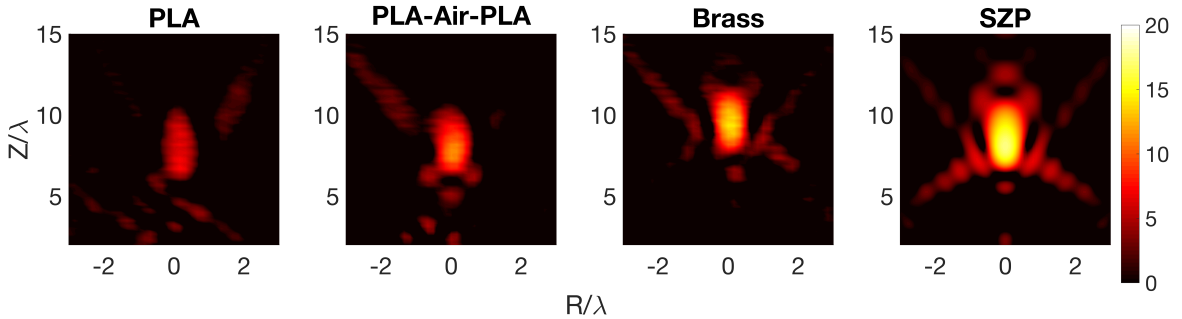

Figure 6. Intensity gain maps for experimental measurements and ideal SZP numerically obtained (FEM).

5. Conclusions

Non-metallic materials can be used for the construction of acoustic lenses. Three alternative materials, compatible with magnetic resonance, have been proposed instead of brass lenses. It has been possible to verify that the higher the impedance contrast of the materials, the higher the intensity gain levels. The PMMA lens has higher intensity level than ABS and PLA ones, because it has a slightly higer impedance contrast value than ABS or PLA. However, the use of an air chamber inside the PLA

lens increases the intensity gain levels, due to the fact that values of impedance contrast less than one means blocking of the waves. PLA is a biocompatible material and is cheaper than PMMA. 3D printers give open field of new lens design MRI compatible. Moreover, since PLA is a biodegradable material, it is a environmental friendly material. This point is important in procedures that generate waste. Nevertheless, the manufacture of PLA lenses require great care because of microporosities that could appear. The appearance of pores can cause water to enter into the lens, drastically reducing the blocking capacity. In addition, polymers such as PLA, ABS or PMMA are more affordable than metal plates. This will lower the costs in the production of HIFU treatment devices based on acoustic lenses. For this reason, PLA is proposed as an MRI compatible material with great potential for therapeutic applications of ultrasound focusing.

Author Contributions: A.U. and C.R. coordinated the theoretical development, participating in the establishment of the theory principles used in this work, as well as in the drafting of the manuscript. D.T.-S. coordinated experimental development. S.C.-I. developed part of the theory used and designed some characterization. E.S.-A. participated in the analysis of the state of art.

Funding: This research was funded by spanish Ministerio de Economía y Competitividad (MINECO) TEC2015-70939-R.

Acknowledgments: This work has been supported by Spanish MINECO (TEC2015-70939-R).

Conflicts of Interest: The authors declare no conflict of interest.

References

1. Li, J.T.; Han, J.F.; Yang, J.H.; Li, T.S. An efficient synthesis of 3, 4-dihydropyrimidin-2-ones catalyzed by NH_2SO_3H under ultrasound irradiation. *Ultrason. Sonochem.* **2003**, *10*, 119–122. [CrossRef]
2. McCann, D.M.; Forde, M.C. Review of NDT methods in the assessment of concrete and masonry structures. *NDT E Int.* **2001**, *34*, 71–84. [CrossRef]
3. Albu, S.; Joyce, E.; Paniwnyk, L.; Lorimer, J.P.; Mason, T.J. Potential for the use of ultrasound in the extraction of antioxidants from Rosmarinus officinalis for the food and pharmaceutical industry. *Ultrason. Sonochem.* **2004**, *11*, 261–265. [CrossRef] [PubMed]
4. Cervera, F.; Sanchis, L.; Sánchez-Pérez, J.V.; Martínez-Sala, R.; Rubio, C.; Meseguer, F.; López, C.; Caballero, D.; Sánchez-Dehesa, J. Refractive acoustic devices for airborne sound. *Phys. Rev. Lett.* **2002**, *88*, 023902. [CrossRef] [PubMed]
5. Li, Y.; Liang, B.; Tao, X.; Zhu, X.F.; Zou, X.Y.; Cheng, J.C. Acoustic focusing by coiling up space. *Appl. Phys. Lett.* **2012**, *101*, 233508. [CrossRef]
6. Welter, J.T.; Sathish, S.; Christensen, D.E.; Brodrick, P.G.; Heebl, J.D.; Cherry, M.R. Focusing of longitudinal ultrasonic waves in air with an aperiodic flat lens. *J. Acoust. Soc. Am.* **2011**, *130*, 2789–2796. [CrossRef] [PubMed]
7. Peng, P.; Xiao, B.; Wu, Y. Flat acoustic lens by acoustic grating with curled slits. *Phys. Lett. A* **2014**, *378*, 3389–3392. [CrossRef]
8. Castiñeira-Ibáñez, S.; Tarrazó-Serrano, D.; Fuster, J.; Candelas, P.; Rubio, C. Polyadic cantor fractal ultrasonic lenses: Design and characterization. *Appl. Sci.* **2018**, *8*, 1389. [CrossRef]
9. Soret, J. Ueber die durch Kreisgitter erzeugten Diffractionsphänomene. *Ann. Phys.* **1875**, *232*, 99–113. [CrossRef]
10. Calvo, D.C.; Thangawng, A.L.; Nicholas, M.; Layman, C.N. Thin Fresnel zone plate lenses for focusing underwater sound. *Appl. Phys. Lett.* **2015**, *107*, 014103. [CrossRef]
11. McDannold, N.; Hynynen, K.; Wolf, D.; Wolf, G.; Jolesz, F. MRI evaluation of thermal ablation of tumors with focused ultrasound. *J. Magn. Resonance Imaging* **1998**, *8*, 91–100. [CrossRef]
12. Drumright, R.E.; Gruber, P.R.; Henton, D.E. Polylactic acid technology. *Adv. Mater.* **2000**, *12*, 1841–1846. [CrossRef]
13. Herrmann, K.H.; Gärtner, C.; Güllmar, D.; Krämer, M.; Reichenbach, J.R. 3D printing of MRI compatible components: Why every MRI research group should have a low-budget 3D printer. *Med. Eng. Phys.* **2014**, *36*, 1373–1380. [CrossRef] [PubMed]

14. Köhler, M.O.; Mougenot, C.; Quesson, B.; Enholm, J.; Le Bail, B.; Laurent, C.; Moonen, C.T.; Ehnholm, G.J. Volumetric HIFU ablation under 3D guidance of rapid MRI thermometry. *Med. Phys.* **2009**, *36*, 3521–3535. [CrossRef] [PubMed]
15. Rocca-Smith, J.R.; Whyte, O.; Brachais, C.H.; Champion, D.; Piasente, F.; Marcuzzo, E.; Sensidoni, A.; Debeaufort, F.; Karbowiak, T. Beyond biodegradability of poly (lactic acid): physical and chemical stability in humid environments. *ACS Sustain. Chem. Eng.* **2017**, *5*, 2751–2762. [CrossRef]
16. COMSOL-Multiphysics. *COMSOL-Multiphysics User Guide (Version 4.3a)*; COMSOL User Guide (Version 4.3a); COMSOL Inc.: Stockholm, Sweden, 2012; pp. 39–40.
17. Kinsler, L.E.; Frey, A.R.; Coppens, A.B.; Sanders, J.V. *Fundamentals of Acoustics*, 4th ed.; John Wiley and Sons: New York, NY, USA, 1999; p. 560.
18. Zienkiewicz, O.C.; Taylor, R.L.; Zienkiewicz, O.C.; Taylor, R.L. *The Finite Element Method*; McGraw-Hill: London, UK, 1977; Volume 36.
19. Castiñeira-Ibáñez, S.; Tarrazó-Serrano, D.; Rubio, C.; Candelas, P.; Uris, A. An ultrasonic lens design based on prefractal structures. *Symmetry* **2016**, *8*, 28. [CrossRef]
20. Tarrazó-Serrano, D.; Rubio, C.; Minin, O.V.; Candelas, P.; Minin, I.V. Manipulation of focal patterns in acoustic Soret type zone plate lens by using reference radius/phase effect. *Ultrasonics* **2019**, *91*, 237–241. [CrossRef] [PubMed]